RSC Advances

PAPER

View Article Online
View Journal | View Issue

Cite this: *RSC Adv.*, 2017, **7**, 52245

Template synthesis of hierarchical porous metal–organic frameworks with tunable porosity†

Chongxiong Duan, ‡ Feier Li,‡ Hang Zhang, Jinqing Li, Xiujun Wang and Hongxia Xi*

Hierarchical porous metal–organic frameworks (HP-MOFs) with tunable porosity are highly valuable for many applications. Here, we developed a versatile solvothermal method to synthesize various HP-MOFs, such as Cu–BTC and ZIF-8, by using an organic amine as the template. The resulting HP-MOF products were characterized by a complementary combination of X-ray powder diffraction, Fourier-transform infrared spectroscopy, scanning electron microscopy, transmission electron microscopy, nitrogen adsorption–desorption isotherms, pore size distributions analysis, thermogravimetric analysis, and density functional theory calculations. The results indicated that the obtained HP-MOF products had high thermal stability and contained multimodal hierarchically porous structures with mesopores or macropores interconnected with micropores. In addition, the porosities of the produced HP-MOFs could be easily tuned by controlling the amount of the template. The introduced organic amine served as the template to direct the formation of mesopores and macropores. Furthermore, the synthesis route is highly versatile as other organic amines (*e.g.*, *N*,*N*-dimethylhexadecylamine and *N*,*N*-dimethyltetradecylamine) can also be used as templates to synthesize HP-MOFs. The method developed in this work may offer a new direction to synthesize various stable HP-MOFs with tunable porosities for a wide range of applications.

Received 9th August 2017
Accepted 23rd October 2017

DOI: 10.1039/c7ra08798e

rsc.li/rsc-advances

Introduction

Metal–organic frameworks (MOFs), which are constructed through the self-assembly of organic ligands with metal ions or clusters, are interesting crystalline materials that can be classified into thousands of types with high surface area, tunable functionality, and permanent porosity.[1–4] They have received considerable attention in the past two decades because of their very promising potential in industrial applications, such as adsorption/separation,[5,6] drug delivery,[7,8] chemical sensing,[9,10] and catalysis.[11,12] Nevertheless, almost all reported MOF materials to date are microporous structures with pore sizes below 2 nm.[13] Although the inherent micropores in MOFs are desirable for reactions owing to their strong affinity for guest molecules,[14,15] they can also hinder the fast diffusion and mass transfer of reactants or products, especially large molecules.[16,17] In addition, micropores are seldom accessible for anchoring molecular catalysts or impregnating catalyst precursors, or for transport of voluminous drug molecules,[18] which greatly limits their application in fine chemical transformations, drug delivery, or nanoparticle formation.[19]

To solve the diffusion and accessibility problems that guest species face in conventional MOFs with micropores, hierarchical porous MOF materials (HP-MOFs; MOFs with micro- and mesopores, or MOFs with micro-, meso-, and macropores) with tunable porosity, such as Cu–BTC,[20] ZIF-8,[21] and Zn–MOF-74,[22] have been successfully synthesized since 2008. The extended pore structures (mesopores or macropores, or both mesopores and macropores) in HP-MOF materials can improve the diffusion rate and facilitate mass transfer of reactants or products. So far, four main methods have been developed to enlarge the pore size of conventional MOFs: ligand extension,[23] post-processing,[24] the use of mixed ligands,[25] and templating.[26] However, smaller mesopore size (<10 nm), volatility, instability, and vulnerable interpenetrating frameworks are almost unavoidable in HP-MOF products synthesized by the ligand-extension method.[14] In addition, the post-processing and mixed-ligand methods tend to generate mesopores with uncontrollable size in the resulting HP-MOFs.[27] For the template method, surfactants (ionic and neutral) or block copolymers are usually used as templates to direct the formation of mesopores in the internal MOF crystals.[16] They can be easily manipulated and are feasible for preparing stable HP-MOFs with controllable porosity.[14,28] For example, cetyltrimethylammonium bromide (CTAB) has been reported as

School of Chemistry and Chemical Engineering, South China University of Technology, Guangzhou 510640, P. R. China. E-mail: cehxxi@scut.edu.cn

† Electronic supplementary information (ESI) available. See DOI: 10.1039/c7ra08798e

‡ These authors contributed equally to this work.

a template that can be used to synthesize stable hierarchical porous Cu–BTC and ZIF-8.[20,29] The triblock copolymers P123 and F127, which are widely applied to synthesize mesoporous zeolites, have also been used as templates to prepare stable HP-MOFs (*e.g.*, Cu–BTC).[30–32] Other new kinds of templates have also been reported for the synthesis of HP-MOFs, such as amphiphilic dodecanoic acid (DDA),[33] *N*-ethyl perfluorooctylsulfonamide (*N*-EtOFSA),[28] and 4-(dodecyloxy)benzoic acid (DBA).[34] However, the species of templates reported to date that can be applied to synthesize HP-MOFs are limited. Therefore, it is highly desirable to extend the species of templates for the preparation of HP-MOFs with tunable porosity.

In this work, we adopted a new surfactant—organic amine—as the template and developed a solvothermal route to synthesize two stable HP-MOFs, Cu–BTC and ZIF-8. The porosity of the HP-MOF materials could be controlled by varying the molar concentration of the template. In addition, the molecular properties of the organic amine were studied based on density functional theory (DFT), with the amine group easily attacked by electrophilic species. Furthermore, a possible mechanism for the template synthesis of HP-MOFs was investigated. Other organic amines (*e.g.*, *N*,*N*-dimethylhexadecylamine and *N*,*N*-dimethyltetradecylamine) could also be used as templates to synthesize hierarchical porous MOFs, demonstrating the versatility of our synthesis method.

Experimental

Synthesis of hierarchical porous Cu–BTC

In a typical synthesis process, 4.5 mmol of $Cu(NO_3)_2 \cdot 3H_2O$ was added in 15 mL of deionized water to obtain solution A. Next, 2.5 mmol of 1,3,5-benzenetricarboxylic acid (H_3BTC) and X (X = 0.45, 2.25, or 4.5) mmol of *N*,*N*-dimethyloctadecylamine were added in 15 mL of anhydrous ethanol; hereafter, this mixture is referred to as solution B. After both solutions were stirred for 0.5 h, solution B was added in solution A, and the mixture was stirred for 1 h. The final gel mixture was transferred into a 100 mL Teflon-lined stainless steel autoclave and heated at 383 K for 24 h. After cooling naturally to room temperature, the solid product was filtered and washed twice with 25 mL of ethanol. To remove the template and solvents trapped in the channels, the solid product was immersed in ethanol four times at 373 K for 48 h, and the final product was dried in an oven at 423 K for 12 h. The resulting products are denoted as Cu–BTC_An (n = 1, 2, 3, where n represents the amount of *N*,*N*-dimethyloctadecylamine, *i.e.*, n = 1 for 0.45 mmol, n = 2 for 2.25 mmol, and n = 3 for 4.5 mmol). For comparison, conventional Cu–BTC was prepared according to a previously reported procedure,[35] and it is denoted as C-Cu–BTC.

Characterization

Powder X-ray diffraction (XRD) patterns were recorded on a diffractometer system (D8 ADVANCE, Bruker AXS) using Ni-filtered Cu-target Kα radiation (40 kV, 40 mA, wavelength λ = 0.15418 nm). XRD patterns of the MOFs were simulated by using the Materials Studio package 5.0 (Materials Studio, BIOVIA), and the crystal structure file was obtained from the Cambridge Crystallographic Data Centre (Cu–BTC for CCDC-112954). Fourier-transform infrared (FTIR) spectra of samples in the form of KBr pellets were recorded on an FTIR spectrometer (Vector 33, Bruker Corporation) with a resolution of 4 cm^{-1}. Scanning electron microscope (SEM; ZEISS Ultra 55, Carl Zeiss) images were obtained at a low loading energy and voltage of 5.0 kV. Transmission electron microscopy (TEM) was performed with an electron microscope (JEM-2100HR, JEOL) operated at 200 kV. N_2 adsorption–desorption data were measured with a surface area and porosity analyzer (ASAP 2460, Micromeritics) at 77 K. All of the samples were outgassed for 6 h at 393 K before the measurements. Thermogravimetric analysis (TGA) of the samples was carried out with a TG analyzer (TG 209, Netzsch) and heated from 298 to 873 K in a N_2 atmosphere at a rate of 5 K min^{-1}.

Calculations

Density functional theory is a very useful tool for understanding molecular properties and describing the behavior of atoms in molecules.[36] The geometry optimization of an organic amine molecule was performed at the DFT Becke three-parameter Lee–Yang–Parr (B3LYP) level using the 6-311+G(d, p) basis set with the Gaussian 09 program.[37] This basis set provides the basis functions for a wide range of organic compounds with accurate molecular geometry and electronic properties.[38,39] In addition, the molecular electrostatic potential (MEP) and frontier molecular orbitals of organic amine were based on the B3LYP method and 6-31+G* basis set.

Results and discussion

Fig. 1a presents the XRD patterns of the hierarchical porous Cu–BTC (Cu–BTC_An (n = 1, 2, 3)) and conventional Cu–BTC (C-Cu–BTC), as well as the simulated pattern from the Materials Studio package 5.0.[40] As shown in Fig. 1a, all diffraction peak positions of Cu–BTC_An (n = 1, 2, 3) are well matched with those of C-Cu–BTC and the simulation data, confirming that the products are crystalline Cu–BTC. However, the XRD patterns of both Cu–BTC_A3 and C-Cu–BTC exhibit somewhat larger (111) peaks,

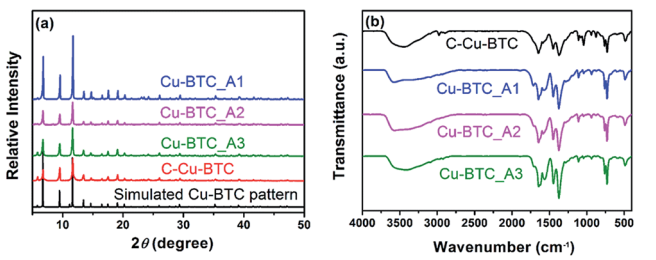

Fig. 1 (a) Powder XRD patterns of C-Cu–BTC and Cu–BTC_An (n = 1, 2, 3) synthesized from solutions containing various molar concentrations of organic amine, and the simulated Cu–BTC XRD pattern; (b) FTIR spectra of the as-synthesized Cu–BTC_An (n = 1, 2, 3) and C-Cu–BTC samples.

most likely because of dehydration and rehydration.[41] In addition, broader XRD peaks are observed in the patterns of Cu–BTC_A*n* than those in the patterns of C-Cu–BTC and the simulation result, which can be attributed to either the small crystallite size or abundance of lattice defects.[42,43] These crystal structures were further studied using FTIR spectroscopy. As shown in Fig. 1b, the FTIR spectra of all Cu–BTC_A*n* samples are in agreement with that of C-Cu–BTC (with major peaks at approximately 1560, 1450, and ~1370 cm^{-1}), which is clearly identified as pure Cu–BTC. In addition, we further compared the FTIR spectra of the Cu–BTC_A*n* ($n = 1, 2, 3$) with those of the C-Cu–BTC samples in a narrow region (1500–1000 cm^{-1}), as shown in Fig. S1.† The FTIR spectrum of Cu–BTC_A*n* was in accord with that of the C-Cu–BTC synthesized without organic amines as the template, and a typical C–N stretching vibration of organic amines (around 1210 cm^{-1}) was absent. These results indicate that the introduced organic amine did not react with organic ligands or metal ions to form other crystals, and similar conclusions were drawn in earlier works of Zhang *et al.*[44] and Nordin *et al.*[45]

The morphologies and porous structures of the as-synthesized MOF products were revealed by SEM and TEM. While the C-Cu–BTC particles had octahedral shapes with smooth surfaces (Fig. S2†), all of the as-synthesized Cu–BTC_A*n* samples consisted of block-shaped particles with disordered pores of 20–100 nm in size between these particles (according to the pore size distribution (PSD, Fig. 3b)), as shown in the SEM images in Fig. 2a–c. The difference between the crystal morphology of C-Cu–BTC and Cu–BTC_A*n* can be attributed to the effect of the introduced template.[16,46,47] In addition, these Cu–BTC_A*n* samples. Furthermore, it can be seen in Fig. 2a–c that all Cu–BTC_A*n* samples exhibit smaller particle sizes (~100 nm) than C-Cu–BTC (~10 μm, Fig. S2†), which is in good agreement with the broader XRD peaks of Cu–BTC_A*n* in Fig. 1a. As expected, high-resolution TEM offered insight into the local structure of the crystalline phases.[48] As shown in Fig. 2d–f, these Cu–BTC_A*n* samples also exhibit similar shapes and pore structures, with dense, uniform nanoflakes randomly stacked together and abundant voids in between. Cao *et al.*[49] and Hirai *et al.*[50] also reported that hierarchical porous structures in MOFs are formed through the aggregation or packing of microporous nanoparticles. Although void structures are clearly observed in all of the Cu–BTC_A*n* samples (Fig. 2), their pore sizes differ depending on the amount of the template used.

The representative N_2 adsorption–desorption isotherms and pore size distributions (PSDs) in Fig. 3 illustrate the porosity of the Cu–BTC_A*n* samples. As shown in Fig. 3a, the isotherms of the three samples represent an intermediate mode between type I and type IV,[26] in which the high uptake of adsorbates at the initial stage confirms the presence of micropores. The apparent hysteresis loop in the relative pressure range between 0.8 and 1.0 indicates the wide size distribution of mesopores,[20,51] but these features do not appear in the isotherm of C-Cu–BTC. These analysis results confirm that micropores and mesopores were present in the Cu–BTC_A*n* products, and similar conclusions were drawn from the works of Bradshaw *et al.*[16] and Sun *et al.*,[26] in which a series of hierarchical porous MOFs were synthesized by a template strategy, and the isotherms of the obtained MOFs showed a sharp increase in the uptake of adsorbates and an apparent hysteresis loop, revealing the formation of both micropores and mesopores. In addition, the isotherms of different Cu–BTC_A*n* samples indicate obvious differences in their adsorption capacities, and the hysteresis loops that vary with the molar concentration of the template indicate the differences in the porosity of the samples.[51] More detailed information regarding the porosity of Cu–BTC_A*n* materials is acquired from the PSDs. As shown in Fig. 3b, in addition to the intrinsic micropores (0.8–0.9 nm in diameter), the as-synthesized Cu–BTC_A*n* contains pores with a broad range of pore sizes from 20 to over 100 nm, including regions of meso- and macroporous regions that are absent in C-Cu–BTC. Although there have been a couple of reports of Cu–BTC with

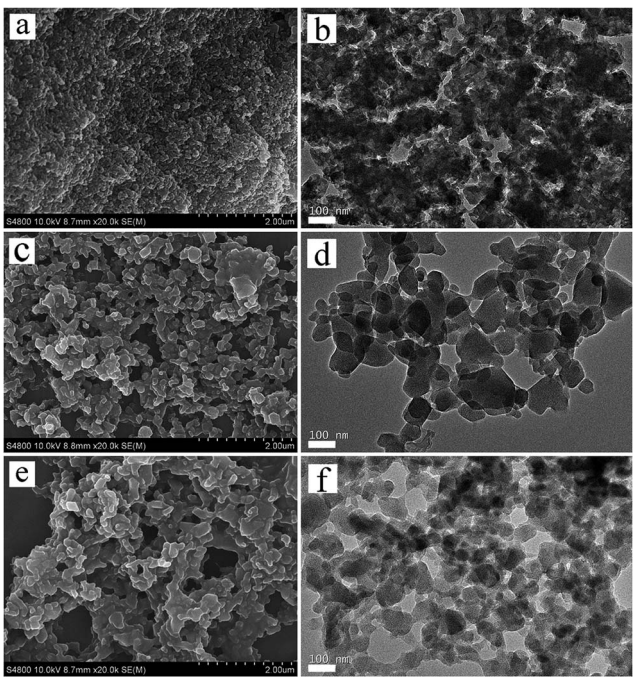

Fig. 2 SEM and TEM images of the hierarchical porous Cu–BTC_A*n* ($n = 1, 2, 3$) materials: (a, b) Cu–BTC_A1; (c, d) Cu–BTC_A2; (e, f) Cu–BTC_A3.

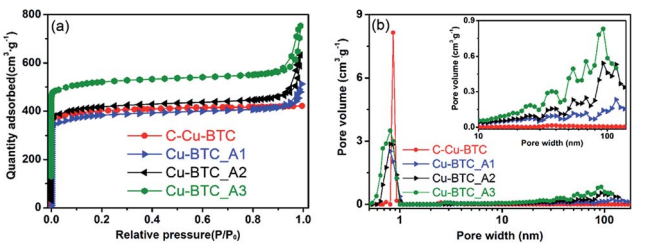

Fig. 3 (a) N_2 adsorption–desorption isotherms and (b) pore size distributions (PSD) of the hierarchical porous Cu–BTC_A*n* ($n = 1, 2, 3$) samples. For show the line shapes more clearly, the isotherms of Cu–BTC_A2 and Cu–BTC_A3 are vertically offset by 20 and 120 $cm^3\ g^{-1}$, respectively.

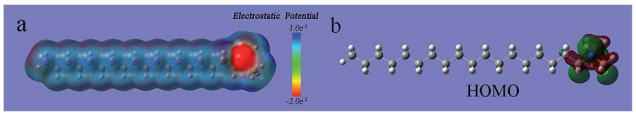

Fig. 4 (a) Molecular electrostatic potential map (MEP); (b) surface of molecular orbital of *N*,*N*-dimethyloctadecylamine (legend of atoms: white = H; gray = C; blue = N).

both micro- and mesopores,[16,52] such hierarchical porous Cu–BTC material with pore diameters encompassing three ranges (micro-, meso-, and macropores) are, to the best of our knowledge, quite rare. Interestingly, the pore volume of Cu–BTC_A*n* increases with increasing template concentration (inset of Fig. 4b), and similar trends can be seen in the summary of data in Table 1. These results not only validate the generation of mesoporosity in the Cu–BTC_A*n* samples, but also indicate that the porosity of hierarchical porous MOFs could be controlled by the amount of template used during synthesis. In addition, the pore size distributions of H-MOFs exhibited consistency when the synthesis is repeated, as shown in Fig. S3.† Furthermore, we achieved the same porosity in the H-MOFs even for scaled-up syntheses using 2 and 10 times the original amounts of the materials, as shown in Fig. S4.†

The porosity properties of the hierarchical porous Cu–BTC_A*n* ($n = 1, 2, 3$) and C-Cu–BTC are summarized in Table 1. All of the Cu–BTC_A*n* samples exhibit lower Brunauer–Emmett–Teller (BET) surface areas (S_{BET}) than C-Cu–BTC, which can be attributed to the increased fraction of meso- and macropores decreasing S_{BET}. Similar conclusions were drawn from the works of Qiu *et al.*,[20] Yue *et al.*,[22] and Huang *et al.*[14] However, all Cu–BTC_A*n* products have much higher total pore volumes (V_t) and mesopore volumes (V_{meso}) than C-Cu–BTC, confirming the generation of mesopores in the Cu–BTC_A*n* samples. In addition, as the amount of template is increased from 0.45 to 4.5 mmol during synthesis, V_t of the MOF products is increased from 0.66 (for Cu–BTC_A1) to 0.81 $cm^3\ g^{-1}$ (for Cu–BTC_A3), and V_{meso} is also increased from 0.19 to 0.31 $cm^3\ g^{-1}$. Moreover, the mesopore diameter is increased from 7.2 to 12.7 nm as the amount of template is increased. Therefore, the porosity of the hierarchical porous MOFs was readily tuned by varying the amount of template added during synthesis.

Thermogravimetric analysis was performed under a N_2 atmosphere to assess the thermal stability of the obtained hierarchical porous Cu–BTC_A*n*. It can be seen from Fig. S5† that the initial stage of weight loss in all samples occurred at 100 °C owing to the evaporation of trapped solvent (*e.g.*, deionized water).[53,54] The second stage of weight loss in Cu–BTC_A*n* was observed at approximately 220 °C, which probably corresponds to the loss of guest molecules in the pore channels.[55,56] As shown in Fig. S5,† the weight of all samples dropped sharply after 300 °C, which can be attributed to the structural decomposition of Cu–BTC_A*n* crystals.[57] The TGA curves of Cu–BTC_A*n* exhibited a consistent trend indicating that the amount of added template had no significant impact on the thermal stability of the hierarchical porous MOFs. In addition, the hierarchical porous MOF products exhibited weight change curves similar to that of C-Cu–BTC during the same thermal treatment, indicating that the as-synthesized hierarchical porous Cu–BTC_A*n* had high thermal stability.

The organic amine molecules used in the present work contained amine groups and alkyl chain moiety, and the molecular electrostatic potential (MEP) of the template was calculated by using the DFT-B3LYP method and the 6-31G* basis set. The negative region (red) of the MEP is related to electrophilic reactivity, and the positive region (blue) to nucleophilic reactivity.[58] As shown in Fig. 4a, the negative region of the *N*,*N*-dimethyloctadecylamine molecule is mainly concentrated on the amine group at the tail end, which represents the most susceptible sites for electrophilic attacks.[59] Fig. 4b shows the distributions of the highest occupied molecular orbital (HOMO) calculated at the B3LYP/6-31G* level for the *N*,*N*-dimethyloctadecylamine molecule. The HOMO energy is directly related to the ionization potential and characterizes the susceptibility of a molecule toward attack by electrophiles.[60] As shown in Fig. 4b, the HOMO is also mainly located in the amine group. The analysis confirms that the amine group of *N*,*N*-dimethyloctadecylamine is easily attacked by electrophilic species. Based on the above findings and results reported in the literature,[16] a possible mechanism for the synthesis of hierarchical porous MOFs by using *N*,*N*-dimethyloctadecylamine as the template is illustrated in Scheme 1. In the initial stages, *N*,*N*-dimethyloctadecylamine formed supramolecular micelles through self-assembly,[61,62] and then H contained in the ligands (H_3BTC) interacted with the amine group of the template because the negative region was mainly concentrated in the tail-end amine group that easily attracted electrophilic species.[60]

Table 1 Porosity properties of the hierarchical porous Cu–BTC_A*n* ($n = 1, 2, 3$) and C-Cu–BTC samples

Samples	S_{BET}[a] [$m^2\ g^{-1}$]	S_{micro}[b] [$m^2\ g^{-1}$]	S_{meso}/S_{micro}[c]	V_t[d] [$cm^3\ g^{-1}$]	V_{meso}[e] [$cm^3\ g^{-1}$]	D_{meso}[f] [nm]
C-Cu–BTC	1399	1313	0.08	0.60	0.05	1.8
Cu–BTC_A1	1231	1026	0.20	0.66	0.19	7.2
Cu–BTC_A2	1325	1074	0.23	0.79	0.29	11.9
Cu–BTC_A3	1351	1080	0.25	0.81	0.31	12.7

[a] S_{BET}: Brunauer–Emmett–Teller (BET) surface area. [b] S_{micro}: micropore surface area calculated using the BET equation. [c] S_{meso}: mesopore surface area calculated using the BET equation. [d] V_t: total pore volume determined by using the adsorption branch of the N_2 isotherm at $P/P_0 = 0.99$. [e] V_{meso}: mesopore volume based on the density functional theory (DFT) method. [f] D_{meso}: mesopore diameter is determined from the local maximum of the BJH distribution of pore diameters obtained in the adsorption branch of the N_2 isotherm.

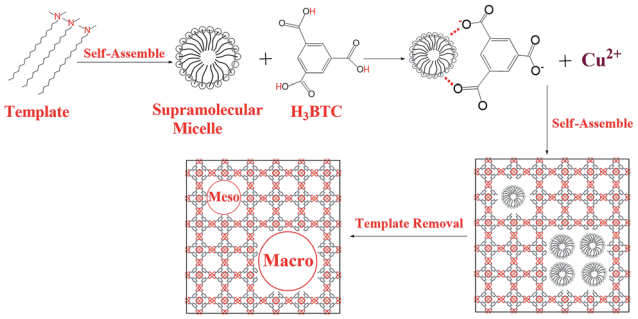

Scheme 1 Map of possible mechanism for the formation of hierarchical porous Cu–BTC materials.

When the $Cu(NO_3)_2$ solution was added, the Cu^{2+} and BTC^{3-} ions began to self-assemble in the presence of the template. Finally, the template was removed to yield mesopores and/or macropores with walls formed by the crystalline microporous MOF.[26] Qiu *et al.*,[20] and Sun *et al.*,[63] also reported a similar mechanism for synthesizing hierarchically structured MOFs by using a template strategy.

Based on the above synthesis mechanism, two other organic amines (*N*,*N*-dimethylhexadecylamine and *N*,*N*-dimethyltetradecylamine, Table S1†) were chosen as templates to synthesize hierarchically porous Cu–BTC, and the resulting products are named as Cu–BTC_B and Cu–BTC_C, respectively (see ESI†). As shown in Fig. S6,† the XRD pattern of the as-synthesized Cu–BTC_B powder matched well with that of C-Cu–BTC, indicating that the obtained product possessed the representative Cu–BTC framework. The isotherm of Cu–BTC_B showed an intermediate mode between type I and type IV, indicating the co-existence of micropores and mesopores (Fig. S7a†). The hierarchical porous structures with micro-, meso-, and macropores of Cu–BTC_B were further confirmed by the PSD, as shown in Fig. S7b.† The SEM and TEM images also exhibited obvious void structures in the Cu–BTC_B powder (Fig. S8†). In addition, Cu–BTC_C also exhibited a hierarchical porous structure (see Fig. S9–11 in ESI for additional data†). These results confirm that other organic amines could also be used for synthesizing HP-MOFs, demonstrating the versatility of the synthesis route.

Hierarchical porous ZIF-8 was also synthesized under hydrothermal synthesis conditions by using organic amine as the template (see ESI†). As shown in Fig. 5a, the XRD pattern of the as-synthesized hierarchical porous ZIF-8_A (the suffix A

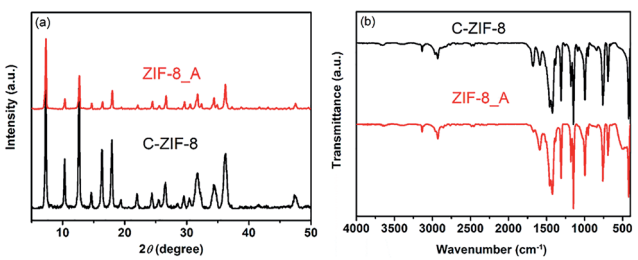

Fig. 5 (a) Powder XRD patterns of ZIF-8_A and C-ZIF-8; (b) FTIR spectra of ZIF-8_A and C-ZIF-8.

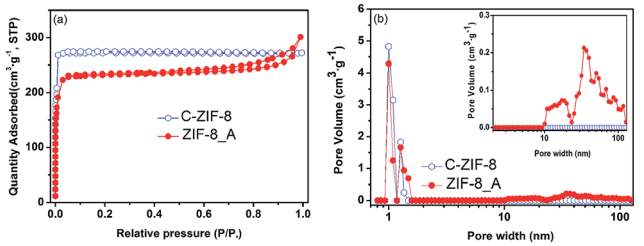

Fig. 6 (a) N_2 adsorption–desorption isotherms and (b) pore size distributions of ZIF-8_A and C-ZIF-8.

means that *N*,*N*-dimethyloctadecylamine was used as the template) agrees with that of conventional ZIF-8 (C-ZIF-8), indicating that the obtained product was crystalline ZIF-8. The FTIR spectrum of ZIF-8_A is in good agreement with that of C-ZIF-8, indicating that ZIF-8_A is phase-pure, as observed in Fig. 5b. The N_2 adsorption–desorption isotherms of ZIF-8_A are a combination of type I and type IV isotherms with an apparent hysteresis loop (Fig. 6a), confirming the co-existence of micropores and mesopores in ZIF-8_A. Furthermore, the PSD of ZIF-8_A reveals that this product possesses mesopores and macropores (Fig. 6b). As shown in Fig. 6a, the hysteresis loop is absent from the isotherm of C-ZIF-8, which means that the conventional material did not contain mesopores and macropores. In addition, the SEM and TEM images (Fig. S12†) show obvious void structures in ZIF-8_A. Thermogravimetric analysis of the hierarchical porous ZIF-8_A and C-ZIF-8 reveals similar weight losses under the same thermal conditions (Fig. S13†), indicating that ZIF-8_A has good thermal stability.

Conclusions

Hierarchical porous MOFs (Cu–BTC and ZIF-8) were successfully synthesized by using a new kind of template. This is the first report of the use of organic amines as templates to synthesize stable HP-MOFs. The resulting MOF products exhibited hierarchical porous structures with micro-, meso-, and macropores, with high pore volume and high thermal stability. More interestingly, the porosity of the hierarchical porous Cu–BTC could be easily tuned by varying the amount of template used in the synthesis of the system. Furthermore, we studied the molecular properties of the organic amine based on the DFT method and investigated a possible synthesis mechanism. In addition, the hierarchical porous Cu–BTC could also be synthesized using other organic amines as the template, demonstrating the versatility of the synthesis approach. This work may open a new window for the template synthesis of various HP-MOFs for a wide range of applications.

Conflicts of interest

There are no conflicts to declare.

Acknowledgements

We gratefully acknowledge the financial support from the National Natural Science Foundation of China (No. 21576094), SRFDP (No. 20130172110012) and Guangdong Natural Science Foundation (No. 2017A030313052).

Notes and references

1 H. K. Chae, D. Y. Siberio-Perez, J. Kim, Y. Go, M. Eddaoudi, A. J. Matzger, M. O'Keeffe and O. M. Yaghi, *Nature*, 2004, **427**, 523–527.
2 H.-L. Jiang, B. Liu, Y.-Q. Lan, K. Kuratani, T. Akita, H. Shioyama, F. Zong and Q. Xu, *J. Am. Chem. Soc.*, 2011, **133**, 11854–11857.
3 F. Luo, M. S. Wang, M. B. Luo, G. M. Sun, Y. M. Song, P. X. Li and G. C. Guo, *Chem. Commun.*, 2012, **48**, 5989–5991.
4 M. Hong, Y. Zhao, W. Su, R. Cao, M. Fujita, Z. Zhou and A. S. C. Chan, *Angew. Chem., Int. Ed.*, 2000, **39**, 2468–2470.
5 Z. Shi, L. Li, Y. Xiao, Y. Wang, K. Sun, H. Wang and L. Liu, *RSC Adv.*, 2017, **7**, 30904–30910.
6 C.-X. Yang, Y.-Z. Zheng and X.-P. Yan, *RSC Adv.*, 2017, **7**, 36297–36301.
7 K. M. L. Taylor-Pashow, J. D. Rocca, Z. Xie, S. Tran and W. Lin, *J. Am. Chem. Soc.*, 2009, **131**, 14261–14263.
8 C.-Y. Sun, C. Qin, C.-G. Wang, Z.-M. Su, S. Wang, X.-L. Wang, G.-S. Yang, K.-Z. Shao, Y.-Q. Lan and E.-B. Wang, *Adv. Mater.*, 2011, **23**, 5629–5632.
9 Z. Z. Lu, R. Zhang, Y. Z. Li, Z. J. Guo and H. G. Zheng, *J. Am. Chem. Soc.*, 2011, **133**, 4172–4174.
10 X. Ma, X. Zhou, Y. Gong, N. Han, H. Liu and Y. Chen, *RSC Adv.*, 2017, **7**, 34609–34617.
11 S. Horike, M. Dincă, K. Tamaki and J. R. Long, *J. Am. Chem. Soc.*, 2008, **130**, 5854–5855.
12 H. Liu, D. Ramella, P. Yu and Y. Luan, *RSC Adv.*, 2017, **7**, 22353–22359.
13 W. Xuan, C. Zhu, Y. Liu and Y. Cui, *Chem. Soc. Rev.*, 2012, **41**, 1677–1695.
14 H. Huang, J.-R. Li, K. Wang, T. Han, M. Tong, L. Li, Y. Xie, Q. Yang, D. Liu and C. Zhong, *Nat. Commun.*, 2015, **6**, 8847.
15 Z. Sun, T. Liao and L. Kou, *Sci. China Mater.*, 2017, **60**, 1–24.
16 D. Bradshaw, S. El-Hankari and L. Lupica-Spagnolo, *Chem. Soc. Rev.*, 2014, **43**, 5431–5443.
17 X. Song, H. Sun, X. Cao, Z. Wang, D. Zhao, J. Sun, H. Zhang and X. Li, *RSC Adv.*, 2016, **6**, 112451–112454.
18 L. Song, J. Zhang, L. Sun, F. Xu, F. Li, H. Zhang, X. Si, C. Jiao, Z. Li and S. Liu, *Energy Environ. Sci.*, 2012, **5**, 7508–7520.
19 N. Klein, I. Senkovska, K. Gedrich, U. Stoeck, A. Henschel, U. Mueller and S. Kaskel, *Angew. Chem., Int. Ed.*, 2009, **48**, 9954–9957.
20 L. G. Qiu, T. Xu, Z. Q. Li, W. Wang, Y. Wu, X. Jiang, X. Y. Tian and L. D. Zhang, *Angew. Chem.*, 2008, **47**, 9487–9491.
21 P. R. Jothi, R. R. Salunkhe, M. Pramanik, S. Kannan and Y. Yamauchi, *RSC Adv.*, 2016, **6**, 21246–21253.
22 Y. Yue, Z.-A. Qiao, P. F. Fulvio, A. J. Binder, C. Tian, J. Chen, K. M. Nelson, X. Zhu and S. Dai, *J. Am. Chem. Soc.*, 2013, **135**, 9572–9575.
23 H. Deng, S. Grunder, K. E. Cordova, C. Valente, H. Furukawa, M. Hmadeh, F. Gándara, A. C. Whalley, Z. Liu and S. Asahina, *Science*, 2012, **336**, 1018–1023.
24 Y. Kim, T. Yang, G. Yun, M. B. Ghasemian, J. Koo, E. Lee, S. J. Cho and K. Kim, *Angew. Chem., Int. Ed.*, 2015, **54**, 13273–13278.
25 B. Liu, Y. Li, S. C. Oh, Y. Fang and H. Xi, *RSC Adv.*, 2016, **6**, 61006–61012.
26 L.-B. Sun, J.-R. Li, J. Park and H.-C. Zhou, *J. Am. Chem. Soc.*, 2011, **134**, 126–129.
27 X. Gu, Z.-H. Lu and Q. Xu, *Chem. Commun.*, 2010, **46**, 7400–7402.
28 Y. Zhao, J. Zhang, B. Han, J. Song, J. Li and Q. Wang, *Angew. Chem., Int. Ed.*, 2011, **50**, 636–639.
29 S. C. Junggeburth, K. Schwinghammer, K. S. Virdi, C. Scheu and B. V. Lotsch, *Chem.–Eur. J.*, 2012, **18**, 2143–2152.
30 L. Peng, J. Zhang, J. Li, B. Han, Z. Xue and G. Yang, *Chem. Commun.*, 2012, **48**, 8688–8690.
31 S. Abedi and A. Morsali, *ACS Catal.*, 2014, **4**, 1398–1403.
32 T.-Y. Ma, H. Li, Q.-F. Deng, L. Liu, T.-Z. Ren and Z.-Y. Yuan, *Chem. Mater.*, 2012, **24**, 2253–2255.
33 S. Diring, S. Furukawa, Y. Takashima, T. Tsuruoka and S. Kitagawa, *Chem. Mater.*, 2010, **22**, 4531–4538.
34 K. M. Choi, H. J. Jeon, J. K. Kang and O. M. Yaghi, *J. Am. Chem. Soc.*, 2011, **133**, 11920–11923.
35 S. S.-Y. Chui, S. M.-F. Lo, J. P. Charmant, A. G. Orpen and I. D. Williams, *Science*, 1999, **283**, 1148–1150.
36 B.-Y. Liu, Z. Liu, G.-C. Han and Y.-H. Li, *Thin Solid Films*, 2011, **519**, 7836–7844.
37 B. Liu, C. Li, Y. Ren, Y. Tan, H. Xi and Y. Qian, *Chem. Eng. J.*, 2012, **210**, 96–102.
38 B. Liu, Y. Tan, Y. Ren, C. Li, H. Xi and Y. Qian, *J. Mater. Chem.*, 2012, **22**, 18631.
39 B. Liu, L. Zheng, Z. Zhu, C. Li, H. Xi and Y. Qian, *Appl. Catal.*, 2014, **470**, 412–419.
40 Y. Ban, Y. Li, X. Liu, Y. Peng and W. Yang, *Microporous Mesoporous Mater.*, 2013, **173**, 29–36.
41 J. Zhao, W. T. Nunn, P. C. Lemaire, Y. Lin, M. D. Dickey, C. J. Oldham, H. J. Walls, G. W. Peterson, M. D. Losego and G. N. Parsons, *J. Am. Chem. Soc.*, 2015, **137**, 13756–13759.
42 T. Ungár, *Scr. Mater.*, 2004, **51**, 777–781.
43 Q. Bao, Y. Lou, T. Xing and J. Chen, *Inorg. Chem. Commun.*, 2013, **37**, 170–173.
44 Z. Zhang, S. Xian, H. Xi, H. Wang and Z. Li, *Chem. Eng. Sci.*, 2011, **66**, 4878–4888.
45 N. A. H. M. Nordin, A. F. Ismail, A. Mustafa, P. S. Goh, D. Rana and T. Matsuura, *RSC Adv.*, 2014, **4**, 33292.
46 L. H. Wee, C. Wiktor, S. Turner, W. Vanderlinden, N. Janssens, S. R. Bajpe, K. Houthoofd, G. Van Tendeloo, S. De Feyter, C. E. Kirschhock and J. A. Martens, *J. Am. Chem. Soc.*, 2012, **134**, 10911–10919.
47 Y. Wu, D. Wang and Y. Li, *Sci. China Mater.*, 2016, **59**, 938–996.
48 Y. Jung, S.-W. Nam and R. Agarwal, *Nano Lett.*, 2011, **11**, 1364–1368.

49 Y. Cao, Y. Ma, T. Wang, X. Wang, Q. Huo and Y. Liu, *Cryst. Growth Des.*, 2016, **16**, 504–510.
50 K. Hirai, S. Furukawa, M. Kondo, H. Uehara, O. Sakata and S. Kitagawa, *Angew. Chem., Int. Ed.*, 2011, **50**, 8057–8061.
51 Y. N. Wu, M. Zhou, B. Zhang, B. Wu, J. Li, J. Qiao, X. Guan and F. Li, *Nanoscale*, 2014, **6**, 1105–1112.
52 R. Kuang, L. Zheng, E. Cottrill, N. Pan, Y. Chi, J. Shi, C. Zhang and X. Chen, *RSC Adv.*, 2016, **6**, 97399–97403.
53 E. V. Perez, K. J. Balkus Jr, J. P. Ferraris and I. H. Musselman, *J. Membr. Sci.*, 2009, **328**, 165–173.
54 J. Cravillon, S. Münzer, S.-J. Lohmeier, A. Feldhoff, K. Huber and M. Wiebcke, *Chem. Mater.*, 2009, **21**, 1410–1412.
55 N. C. Jeong, B. Samanta, C. Y. Lee, O. K. Farha and J. T. Hupp, *J. Am. Chem. Soc.*, 2012, **134**, 51–54.
56 Aarti, S. Bhadauria, A. Nanoti, S. Dasgupta, S. Divekar, P. Gupta and R. Chauhan, *RSC Adv.*, 2016, **6**, 93003–93009.
57 N. Al-Janabi, P. Hill, L. Torrente-Murciano, A. Garforth, P. Gorgojo, F. Siperstein and X. Fan, *Chem. Eng. J.*, 2015, **281**, 669–677.
58 B. Liu, Y. Tan, Y. Ren, C. Li, H. Xi and Y. Qian, *J. Mater. Chem.*, 2012, **22**, 18631–18638.
59 N. Okulik and A. H. Jubert, *Internet Electron. J. Mol. Des.*, 2005, **4**, 17–30.
60 K. F. Khaled, S. A. Fadl-Allah and B. Hammouti, *Mater. Chem. Phys.*, 2009, **117**, 148–155.
61 C. K. Harnett, K. M. Satyalakshmi and H. G. Craighead, *Appl. Phys. Lett.*, 2000, **76**, 2466–2468.
62 W. Li and D. Zhao, *Chem. Commun.*, 2013, **49**, 943–946.
63 L. B. Sun, J. R. Li, J. Park and H. C. Zhou, *J. Am. Chem. Soc.*, 2012, **134**, 126–129.